PAPER • **OPEN ACCESS**

Numerical and experimental investigation of an auxetic piezoelectric energy harvester with frequency self-tuning capability

OPEN ACCESS
IOP Publishing
Smart Materials and Structures
Smart Mater. Struct. **33** (2024) 055022 (18pp)
https://doi.org/10.1088/1361-665X/ad3bfe

Numerical and experimental investigation of an auxetic piezoelectric energy harvester with frequency self-tuning capability

Huili Zhang[1], Shun Chen[2], Mahmoud Karimi[3], Binghao Li[1,*], Serkan Saydam[1] and Mahbub Hassan[4]

[1] School of Minerals and Energy Resources Engineering, The University of New South Wales (UNSW Sydney), Kensington, New South Wales 2052, Australia
[2] School of Mechanical and Manufacturing Engineering, The University of New South Wales (UNSW Sydney), Kensington, New South Wales 2052, Australia
[3] Centre for Audio, Acoustics and Vibration, University of Technology Sydney, Sydney, Australia
[4] School of Computer Science and Engineering, The University of New South Wales (UNSW Sydney), Kensington, New South Wales 2052, Australia

E-mail: binghao.li@unsw.edu.au

Received 4 December 2023, revised 5 March 2024
Accepted for publication 8 April 2024
Published 17 April 2024

Abstract

To deal with the limited availability of long-lasting power sources for sensor nodes in industrial environments, a novel piezoelectric energy harvester with high efficiency and a wide working bandwidth was designed to harvest broadband and random vibrations from the ambient environment. The developed energy harvester adopts a doubly clamped piezoelectric beam with a peanut-shaped auxetic structure to improve the power output. It also incorporates a sliding proof mass for frequency self-tuning, enabling a wider working bandwidth. As the doubly clamped beam exhibits geometry nonlinearity under large vibration amplitudes, the power output of the energy harvester can be further enhanced in the frequency self-tuning process. Finite element simulations are conducted to evaluate the impact of the auxetic structure and the position of the proof mass on the performance of the energy harvester. Experiments are performed to examine the energy harvesting performance of the proposed energy harvester. Under an excitation acceleration of 0.3 g, the use of the sliding proof mass widens the working bandwidth of the auxetic energy harvester (AEH) by 9 Hz, with the maximum root mean square output power of AEH reaching 18.78 μW, which is much higher than that of the plain energy harvester (PEH) or the AEH with a fixed proof mass. The developed energy harvester can successfully power a wireless temperature and humidity sensor node based on the vibration produced by a centrifuge, which demonstrates the practical feasibility of the proposed energy harvester for industrial applications.

Keywords: vibration energy harvesting, piezoelectric, auxetic structure, frequency self-tuning

* Author to whom any correspondence should be addressed.

1. Introduction

Internet of things (IoT) has gained increasing attention in recent years due to its contribution to the safety and productivity in industrial production [1]. Industrial IoT (IIoT) is an interconnected network that enables connectivity and interaction between industrial machines by using various types of sensors [2]. However, the lack of long-term sustainable power supplies for sensors limits the adoption of IoT systems in the industry [3]. Although the advancement of low-power technology has significantly reduced the power consumption of sensors, the batteries in sensors still require routine replacement, which can be extremely difficult for vast sensors installed in hard-to-reach areas [4].

As an alternative to batteries with limited lifespans, vibration energy harvesting is a promising solution for powering standalone low-power IoT sensors because vibration is one of the most ubiquitous and sustainable energy sources in industrial environments. Vibration energy harvesters convert ambient vibrations into electricity mainly based on piezoelectric [5], electromagnetic [6], and electrostatic mechanisms [7]. Among these approaches, the piezoelectric energy harvesting method has been widely investigated for developing self-powered sensors due to its advantages of high energy density [8], simple structure [5], and ease of integration into a micro-device [3]. A conventional linear piezoelectric energy harvester is designed to operate at its resonance frequency. Once frequencies of vibration sources slightly deviate from the resonance frequency of the energy harvester, the power output of the energy harvester would decrease significantly [9]. Since vibrations available in industrial environments are characterised by a broad and random frequency spectrum, it is essential to design a piezoelectric vibration energy harvester with a wide working bandwidth and high power output to supply *in-situ* sensors for industrial applications.

Various techniques have been proposed to yield the working bandwidth of the piezoelectric energy harvester, including multi-frequency harvesting, nonlinearity and frequency tuning mechanisms. A multi-frequency system can be realised by using an array of piezoelectric energy harvesters with different resonance frequencies [10, 11], or by designing a piezoelectric energy harvester with multiple closely spaced vibration modes to scavenge energy from different modes of vibration [12, 13]. Therefore, multi-frequency energy harvesters are always bulky and require complex geometric designs and optimisations. The nonlinearity technique enables piezoelectric energy harvesters to harvest more energy under off-resonance conditions [14]. Nonlinear energy harvesters can be designed by introducing nonlinear forces (e.g. preload [15], mechanical stress [16] and magnetic force [17]) and nonlinear geometries (e.g. M-shaped [18] and L-shaped [19] beam structures). Therefore, nonlinear energy harvesters can be achieved by incorporating auxiliary components, such as stoppers and magnets, to provide nonlinear restoring forces. Alternatively, novel structural designs may be required to induce geometric nonlinearity in the piezoelectric beam under large deformations [20–23].

Frequency tuning is another approach for broadening the working bandwidth of the piezoelectric energy harvester which aims to alter the resonance frequency of the energy harvester during its vibrating process. Active frequency tuning technique consumes additional energy to monitor the working condition of the energy harvester and tune the natural frequency of system by actively modulating structure stiffness [24–28]. In contrast, an energy harvester with passive frequency tuning capability can automatically adapt its resonance frequency to match the excitation frequency without additional energy consumption and human interventions by using a beam-slider structure. The slider could autonomously move along the vibrating beam, thereby shifting the natural frequency of the system [29]. Lan *et al* [30] proposed a cantilever beam-based piezoelectric energy harvester with a sliding proof mass, increasing the working bandwidth of the energy harvester by more than 11 Hz at an excitation acceleration of 1.5 g. Yu *et al* [31] developed a nonlinear cantilever energy harvester incorporating two magnets and a free movable slider. Two magnets were employed at the free end of the beam and on the clamp to arouse the hardening nonlinearity. The slider moved along the beam to ensure that the energy harvester always attain the high energy orbit. Another of their studies [32] indicated the slider could also help the doubly clamped beam capture high energy orbit when the beam exhibited hardening nonlinearity. Miller *et al* [33] experimentally investigated the passive self-tuning performance of a beam-slider resonator that was composed of a clamped-clamped beam and a sliding proof mass. This resonator was capable of passive self-tuning in a wide frequency range regardless of size scale and manufacturing materials. Inspired by this phenomenon, Shin *et al* [34] designed an energy harvester with a doubly clamped piezoelectric beam and a mobile proof mass for broadband energy harvesting, achieving a frequency tuning range of 35 Hz at an excitation acceleration of 0.5 g. The feasibility of this energy harvester for industry applications was validated through the energy harvesting test on a rotary pump.

To augment the power output of the piezoelectric energy harvester, a variety of novel beam geometrical designs have been proposed to replace conventional rectangular cantilevers. Baker *et al* [35] designed a piezoelectric energy harvester that bonded piezoelectric material on a trapezoidal-shaped cantilever beam, resulting in a 30% higher power density than a rectangular counterpart at an excitation acceleration of 4 g. Dietl and Garcia [36] investigated the performance of piezoelectric energy harvesters with three types of beams (i.e. rectangular, linear tapered and reverse tapered beams). They optimised beam structures by varying beam geometrical parameters and tip mass to gain the maximum power output at constant or variable amplitude base excitations. The study conducted by Ayed *et al* [37] showed that the piezoelectric energy harvester with a symmetric quadratic-shaped beam could double the power output compared to the rectangular one.

The auxetic concept also shows great potential for enhancing the power density of piezoelectric energy harvesters. This is attributed to the ability of auxetic structures to generate advantageous lateral forces on piezoelectric materials, which enable both d_{31} and d_{32} operation modes can contribute to power generation [38]. Besides, the introduction of the auxetic structure can increase the magnitude of the

stress, thereby enhancing polarisation to improve the power output [39]. Tabak *et al* [39] thoroughly reviewed the design of piezoelectric energy harvesters based on various auxetic structures. Ebrahimian *et al* [40] numerically and experimentally demonstrated that the auxetic structure could effectively reduce the resonance frequency and increase the power output of the piezoelectric energy harvester. Sadikbasha *et al* [41] proposed a cantilever-based piezoelectric energy harvester with an auxetic hexachiral structure. The power output of the energy harvester can be improved either by replacing the plain substrate with a hexachiral substrate or by adding an additional hexachiral patch on the plain beam. Fang *et al* [42] introduced an auxetic hexagonal pattern to the substrate of a vortex-induced energy harvester with monostable softening behaviour to enhance the power output. Tikariha *et al* [43] investigated the performance of the auxetic energy harvester (AEH) with three types of auxetic structures via finite element modelling (FEM). The results indicated that the energy harvester with an elliptical hole-shaped substrate achieved a higher power output compared to its counterpart with re-entrant or s-shape auxetic structures. Xie *et al* [44] mounted a polyvinylidene fluoride (PVDF) film on the surface of the auxetic cementitious cellular composites to harvest strain energy when subjected cyclic loading. Chen *et al* [45] designed a piezoelectric energy harvester based on a doubly clamped beam with auxetic structures. This harvester included two re-entrant hexagonal honeycomb auxetic arrays located on both ends of the beam and covered by two piezo ceramics. Experimental results indicated that the auxetic structure could increase the power output of the energy harvester by 173% at 0.1 g constant acceleration. Their subsequent studies demonstrated that the power density of an AEH could be further improved by increasing the number of unit cells in an auxetic array [46] and by using gradient auxetic structures [47]. Furthermore, Chen *et al* [38, 39] mentioned that the nonlinearity of the doubly clamped beam could be leveraged to broaden the working bandwidth of the energy harvester. However, capturing the high power output of nonlinear energy harvesters remains a challenging problem due to the coexistence of low and high energy orbits in the system caused by the hysteresis behaviour of the vibrating beam [48]. To ensure the stability of beam vibration at the high energy orbit, various methods such as load perturbation [49] and mechanical impact [50] have been proposed to address this issue.

Given that the previous researchers have exclusively focused on investigating the application of the auxetic structure and the sliding mass on piezoelectric energy harvesters separately, this paper presents the development of a novel piezoelectric energy harvester that integrates passive frequency self-tuning technique and auxetic concept to simultaneously improve the power output and working bandwidth of the energy harvester. The natural frequency and deformation of the energy harvester are evaluated through the FEM. The influence of the auxetic structure on power generation and the frequency self-tuning capability of the sliding proof mass are experimentally investigated. Parametric studies are also conducted to analyse the impact of parameters of the sliding proof mass on vibration energy harvesting. Furthermore, the practical feasibility of the developed energy harvester for industrial applications has been demonstrated by successfully powering a wireless temperature and humidity sensor node.

2. Design, fabrication and working principle

2.1. Energy harvester design and fabrication

The fabricated prototype of the proposed piezoelectric energy harvester is shown in figure 1(a). It consists of a doubly clamped substrate with auxetic structure, a piezoelectric film, and a sliding proof mass. To ensure the smooth movement of the sliding proof mass, the geometric corners of the auxetic substrate should be minimised. Therefore, a peanut-shaped auxetic pattern adapted from the literature [51] is evenly fabricated on the 301 stainless steel beam using laser cutting. Then, a commercial off-the-shelf piezoelectric film (LDT4-028K/L) is bonded to the auxetic substrate through the epoxy adhesive. The piezoelectric film has a total thickness of 157 μm, comprising a PVDF piezoelectric layer (28 μm), a laminated polyester sheet (77 μm), and a protective polyester coating (52 μm). The length, width, and thickness of the composite piezoelectric beam are 171 mm, 22 mm, and 0.8 mm, respectively (figures 1(b) and (c)). Note that although piezoelectric ceramics such as lead zirconate titanate (PZT) are commonly used for vibration energy harvesting due to their higher power density [30, 40, 45, 46], they are brittle and lack of robustness under large displacement. As a result, the flexible PVDF film is applied in this design.

The auxetic structure can be regarded as an array of unit cells with peanut-shaped holes. The geometry of the peanut-shaped hole is determined by two small circles and two large circles tangent to them, as depicted in figure 1(c). The sliding proof mass comprises four pieces of metal, manufactured from 6063 aluminium alloy and engineering steel, and is assembled with bolts and nuts (figure 1(a)). The dimensions of the sliding proof mass are shown in figure 1(d). There is a gap at the centre of the proof mass with a gap size of 1 mm, which allows the proof mass to freely move along the piezoelectric beam. In order to avoid the sliding proof mass being stuck on the piezoelectric beam, the width of the gap (22.3 mm) is slightly wider than that of the piezoelectric beam.

2.2. Auxetic structure

Instead of using a conventional plain substrate, the proposed piezoelectric energy harvester utilises a peanut-shaped auxetic structure on the substrate to boost its power output. On the one hand, the auxetic structure has a negative Poisson's ratio, which is characterised by lateral expansion (along x axis) under a longitudinal tension force (along y axis), as shown in figure 2. In this case, the lateral and longitudinal strains in the auxetic substrate have the same sign, showing opposite behaviour compared to a normal plain substrate. For a piezoelectric energy harvester operating in bending mode, the maximum power output of the energy harvester is equally influenced by both average lateral strain $\overline{\varepsilon_{xx}}$ and average longitudinal strain $\overline{\varepsilon_{yy}}$ in the piezoelectric film (as expressed in equation (1) [47]).

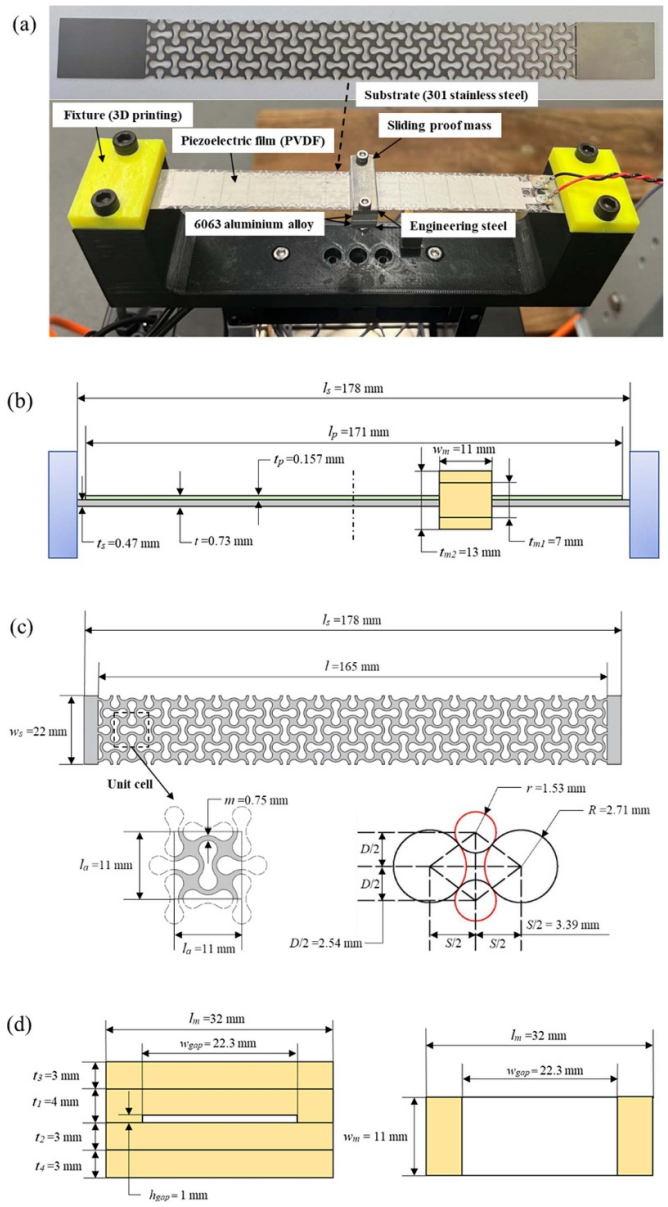

Figure 1. Proposed piezoelectric energy harvester: (a) fabricated prototype of the energy harvester; (b) dimensions of the energy harvester (front view); (c) dimensions of the substrate with a peanut-shaped auxetic structure; (d) dimensions of the sliding proof mass.

In an AEH, negative $\overline{\varepsilon_{xx}}$ can be reduced or even have the same sign as $\overline{\varepsilon_{yy}}$ due to the advantageous lateral force exerted by the auxetic structure.

$$\text{Maximum Power} \propto \left(\overline{\varepsilon_{xx}} + \overline{\varepsilon_{yy}}\right)^2 \tag{1}$$

On the other hand, compared to the plain substrate, the substrate with an auxetic structure can lead to higher stress in the piezoelectric film, thereby enhancing the power output. According to the constitutive equations of piezoelectric effect (equations (2) and (3)) [52], an increase in the stress T in the piezoelectric material contributes to the rise of the electrical displacement D. Therefore, the power output of the piezoelectric energy harvester can be significantly enhanced by the introduced auxetic structure owing to the above-mentioned two advantages.

$$D = dT + \varepsilon E \text{ (Direct effect)} \tag{2}$$

$$X = sT + dE \text{ (Converse effect)} \tag{3}$$

where D is the electrical displacement, d is the piezoelectric coefficient, T is the mechanical stress, ε is the dielectric constant, E is the electric field, X is the mechanical strain, and s is the mechanical compliance.

2.3. Passive frequency self-tuning mechanism

Since vibration frequency levels of common industrial machinery are relatively low (e.g. the dominant frequency of a water pump is 49.5 Hz [53]), in this case, only the first mode of vibration of the proposed doubly clamped beam-based energy harvester is suitable for vibration energy harvesting. The passive frequency self-tuning mechanism of the proposed energy harvester is depicted in figure 3. Initially, the proof mass is placed at the side of the piezoelectric beam. Then, an external constant excitation is applied to the energy harvester with a frequency of f_1. If the vibrating beam can provide sufficient inertia force to the proof mass and the excitation frequency f_1 is within the frequency self-tuning range, the proof mass will autonomously move towards the centre of the beam. During this process, the vibration amplitude of the beam will gradually increase, leading to the occurrence of the hardening nonlinearity in the doubly clamped beam. As a result, the proof mass will not stop at the position where the modulated natural frequency of the energy harvester (as a linear system) matches the excitation frequency. Instead, the proof mass will stop near the centre of the beam to attain a larger vibration amplitude due to the existence of geometric nonlinearity and friction force during the sliding process [54]. Overall, the passive frequency self-tuning behaviour can be attributed to the interaction between the vibrating beam and the sliding proof mass. Specifically, the vibrating beam drives the motion of the proof mass. Consequently, this motion results in the change in the mass distribution of the system, which in turn alters the dynamic response of the vibrating beam. To quantify the frequency self-tuning capability realised by a sliding proof mass, Kim *et al* [55] presented a comprehensive mathematical model of the piezoelectric energy harvester with a doubly clamped plain beam and a sliding proof mass based on extended Hamilton principle by considering the nonlinear dynamics of the doubly clamped beam. However, the motion of the proposed energy harvester cannot be accurately expressed by analytical calculations due to the introduction of the auxetic structure. The mode shape of the proposed energy harvester is more complicated than its plain counterpart, and the cross sections of the substrate with the auxetic structure are not uniform due to the presence of hollows [46].

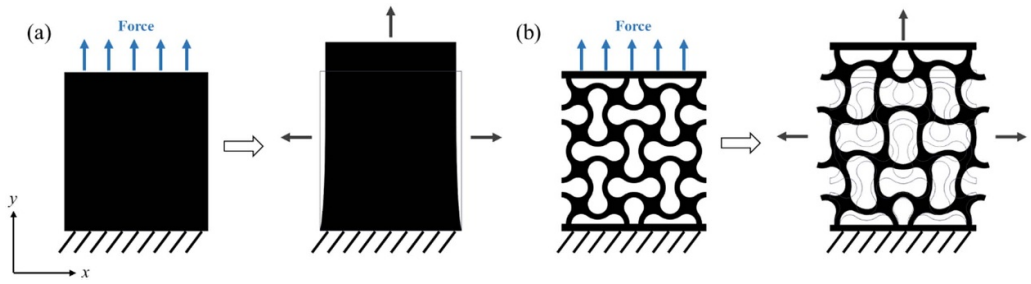

Figure 2. Deformation shapes of (a) the plain structure and (b) the peanut-shaped auxetic structure (2 × 2 unit cells) under longitudinal tension (along *y* axis).

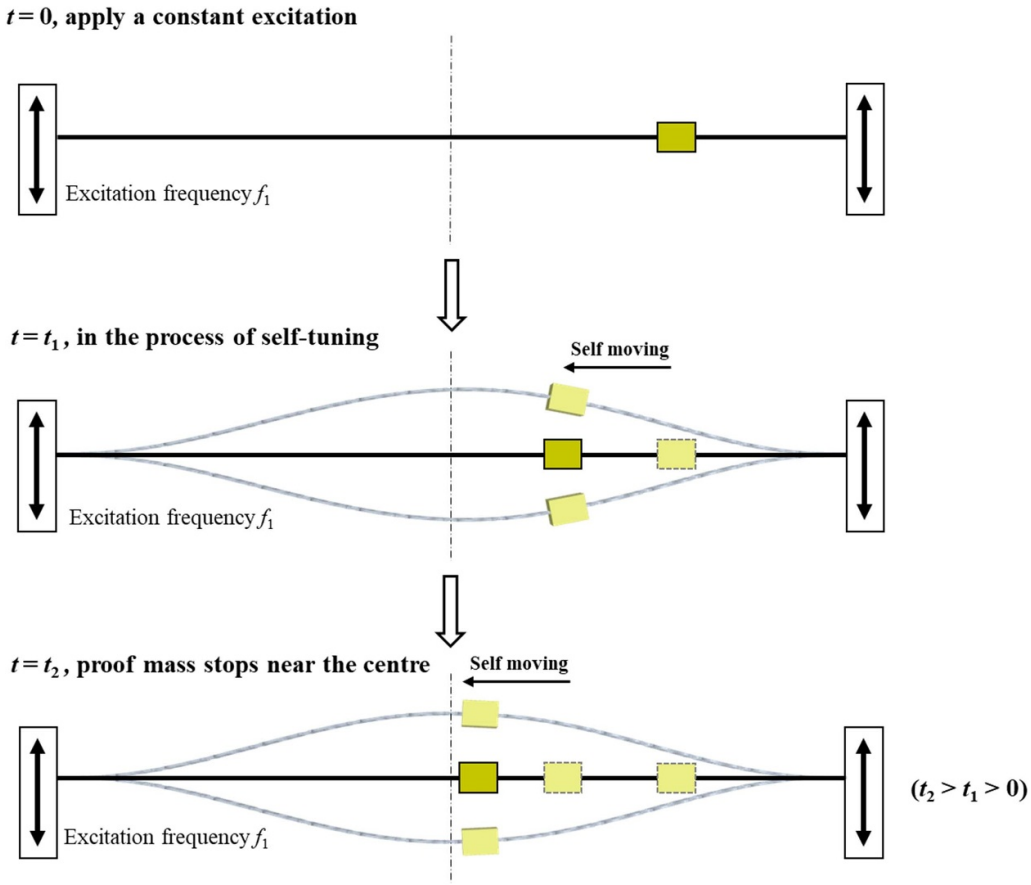

Figure 3. Schematic illustration of frequency self-tuning of the doubly clamped beam-based energy harvester through passive adjustment of the sliding proof mass position.

3. Numerical methodology and experimentation

3.1. FEM

FEM is conducted using COMSOL Multiphysics 5.6, which couples electrostatic physics, electrical circuit and solid mechanics, to estimate the eigenfrequencies of the energy harvester with a fixed proof mass and investigate the effect of the auxetic structure. As shown in figure 4(a), the finite element model of the proposed energy harvester consists of an auxetic substrate with fixed boundary conditions at both ends, a PVDF piezoelectric layer sandwiched between two polyester sheets for power generation, an epoxy layer with the same auxetic pattern as the substrate to bond the piezoelectric film to the substrate, and a proof mass fixed on the piezoelectric beam. To simplify the model, the bolts and nuts on the proof mass are ignored. However, since the weight of the bolt and nuts has a significant influence on the natural frequency of the energy harvester, the density of the proof mass 1 is assumed to be the same as the aluminium alloy 6063, while the density of the proof mass 2 is calculated based on the weight of the proof mass used in the experiments. Besides, considering the imperfect bonding caused by the adhesive, substrate–adhesive–polyester interfaces are modelled as thin elastic layers with a bonding strength of 200 GN m^{-3} [56], and the damping ratio of the system is assumed to be a single isotropic

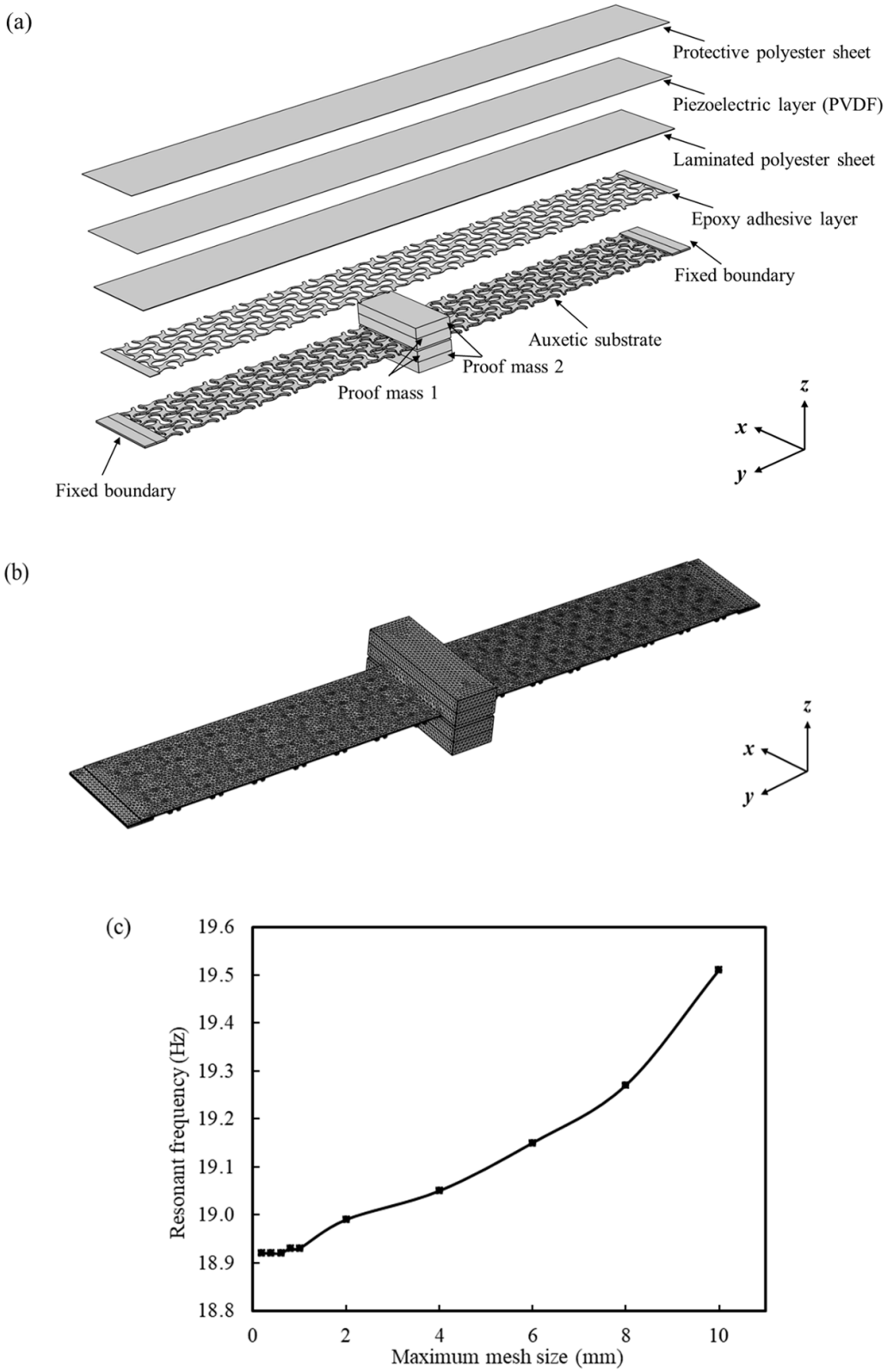

Figure 4. Finite element model of the proposed auxetic energy harvester: (a) exploded view of the energy harvester; (b) mesh configuration of the energy harvester; (c) effect of the maximum mesh size on the natural frequency of the energy harvester.

loss factor with a value of 0.001 [40]. The computational mesh configuration of the proposed AEH is shown in figure 4(b). To characterise the geometry of the auxetic piezoelectric beam, a combination of free triangular mesh and swept meshing are employed to build the mesh of the auxetic piezoelectric beam, while the proof mass is meshed using free tetrahedral mesh

Table 1. Geometrical parameters of the energy harvesters in the modelling.

Component	Parameter	Symbol	Value	Unit
Piezoelectric layer	Length	l_p	171	mm
	Width	w_p	22	mm
	Thickness	t_p	0.028	mm
Laminated polyester sheet	Length	l_1	171	mm
	Width	w_1	22	mm
	Thickness	t_1	0.077	mm
Protective polyester coating	Length	l_2	171	mm
	Width	w_2	22	mm
	Thickness	t_2	0.052	mm
Substrate	Length	l_s	178	mm
	Width	w_s	22	mm
	Thickness	t_s	0.47	mm
Auxetic structure	Radius of two small circle	r	1.53	mm
	Radius of two large circles	R	2.71	mm
	Centroid distance of two small circles	D	5.08	mm
	Centroid distance of two large circles	S	6.78	mm
	Distance between peanut-shaped holes	m	0.75	mm
	Side length of the unit cell	l_a	11	mm
	Total length of the auxetic pattern	l	165	mm
Epoxy adhesive layer	Length	l_e	171	mm
	Width	w_e	22	mm
	Thickness	t_e	0.1	mm
	Bonding strength	k	200	GN m^{-3}
Proof mass (four pieces)	Length	l_m	32	mm
	Width	w_m	11	mm
	Thickness	t_m	3	mm

due to its good adaptability. To achieve precise simulation results within a reasonable computational time, natural frequency of the energy harvester with a proof mass fixed at the centre of the piezoelectric beam is initially calculated to determine the maximum size of the mesh. As depicted in figure 4(c), the natural frequency of the energy harvester shows little sensitivity to the maximum mesh size when it is smaller than 1 mm. Consequently, the maximum mesh size is set at 1 mm. In this configuration, the proposed finite element model comprises 77 391 mesh vertices and a total of 168 384 elements. As a comparison, FEM is also performed to analyse the behaviour of a conventional piezoelectric energy harvester with a plain substrate. The geometrical parameters and material properties of AEH and plain energy harvester (PEH) for FEM are summarised in tables 1 and 2, respectively.

To facilitate the investigation of the performance of the auxetic structure, the proof mass is fixed at the centre of the piezoelectric beam. The modal analysis is conducted to determine the eigenfrequencies of the energy harvester. A sinusoidal body load equivalent to a constant vibration of 0.3 g acceleration [40] at the first eigenfrequency is applied to the energy harvester along the z axis. Since the doubly clamped piezoelectric beam of the energy harvester has a thin thickness and exhibits large deflection when subject to an excitation acceleration of 0.3 g, the impact of geometric nonlinearity should be considered. Besides, in order to explore the effect of the position of the proof mass on the natural frequency of the AEH, the first eigenfrequency of the AEH is calculated by varying the position of the proof mass fixed on the piezoelectric beam.

3.2. Experimental setup

To validate the design concept, an experimental setup is organised to investigate the performance of the proposed piezoelectric energy harvester. As shown in figure 5(a), the energy harvester is vertically mounted on a vibration shaker (APS 113 ELECTRO-SEIS) to be excited by harmonic excitations. The shaker is driven by a power amplifier (APS 125) whose input signal is sourced from a function generator. The vibration frequency and amplitude of the shaker can be manually adjusted to ensure that provided excitation is at the desired level. An accelerometer (Brüel & Kjær 4507-B) is attached to the U-shape fixture to measure the base acceleration generated by the shaker. Two data acquisition modules (DAQ NI-9229 and NI-9234) are used to measure the voltage signal generated by the energy harvester and the acceleration signal measured by the accelerometer, respectively. Simultaneously, these two data acquisition units are connected to the computer, where the measured voltage and acceleration signals can be displayed

Table 2. Material properties of the energy harvesters in the modelling.

Component	Parameter	Symbol	Value	Unit
Piezoelectric element (PVDF)	Density	ρ_{p}	1780	kg m^{-3}
	Compliance matrix	s_{11}^{E}	3.78×10^{-10}	1 Pa
		s_{12}^{E}	-1.48×10^{-10}	1 Pa
		s_{13}^{E}	-1.72×10^{-10}	1 Pa
		s_{22}^{E}	3.78×10^{-10}	1 Pa
		s_{23}^{E}	-1.72×10^{-10}	1 Pa
		s_{33}^{E}	1.09×10^{-9}	1 Pa
		s_{44}^{E}	1.11×10^{-9}	1 Pa
		s_{55}^{E}	1.11×10^{-9}	1 Pa
		s_{66}^{E}	1.43×10^{-9}	1 Pa
	Coupling matrix	d_{31}	2.3×10^{-11}	C/N
		d_{32}	1.48×10^{-12}	C/N
		d_{33}	-3.3×10^{-11}	C/N
	Relative permittivity	ε_{11}	7.4	—
		ε_{22}	9.3	—
		ε_{33}	12.0	—
Polyester sheet	Density	ρ_1	1780	kg m^{-3}
	Poisson's ratio	ν_1	0.2	—
	Young's modulus	E_1	3.5	GPa
Substrate (301 stainless steel)	Density	ρ_{s}	7930	kg m^{-3}
	Poisson's ratio	ν_{s}	0.3	—
	Young's modulus	E_{s}	195	GPa
Epoxy	Density	ρ_{a}	1250	kg m^{-3}
	Poisson's ratio	ν_{a}	0.35	—
	Young's modulus	E_{a}	1.0	GPa
Proof mass 1 (aluminium alloy 6063)	Density	ρ_{m}	2700	kg m^{-3}
	Poisson's ratio	ν_{m}	0.33	—
	Young's modulus	E_{m}	69	GPa
Proof mass 2 (engineering steel)	Density	ρ_{m}	8200	kg m^{-3}
	Poisson's ratio	ν_{m}	0.3	—
	Young's modulus	E_{m}	200	GPa

and recorded by the NI SignalExpress software (figure 5(b)). Note that the measured output voltage is slightly lower than the open-circuit voltage due to the inherent 1 MΩ resistance of the data acquisition module NI-9229. Besides, the piezoelectric film is connected to a resistance box to measure the power output of the energy harvester with different resistances.

4. Results and discussion

4.1. Modal analysis results

As shown in figure 6, the first four eigenfrequencies of the AEH with a proof mass fixed at the centre of the piezoelectric beam are simulated to be 18.93 Hz, 65.56 Hz, 120.82 Hz and 248.57 Hz, respectively. Among four mode shapes, only the first mode of vibration of the AEH can be utilised for vibration energy harvesting in the proposed energy harvester design because this mode enables the sliding proof mass to move smoothly along the vibrating beam for passive frequency self-tuning. Besides, the first eigenfrequency of the PEH is found to be 36.44 Hz, which is significantly higher than that of the proposed AEH. This decrease in the natural frequency of the AEH can be attributed to the lower stiffness of the auxetic substrate in comparison to the plain substrate. Therefore, the introduction of the auxetic can considerably reduce the natural frequency of the energy harvester. The variation of the natural frequency of the AEH with the position of fixed proof mass is shown in figure 7. Despite minor discrepancies, FEM results match well with experimental results. The experimental results indicate that the natural frequency of the AEH exponentially increases from 18.0 to 48.3 Hz, as the proof mass moves from the centre of the piezoelectric beam to the fixed end. This implies that the position of the proof mass significantly affects the dynamic behaviour of the energy harvester.

4.2. Effect of the auxetic structure

To investigate the influence of auxetic structure on the deformation of the piezoelectric beam, finite element simulations were conducted to analyse the displacement distributions of the substrate covered by the piezoelectric layer, as well as the stress and strain distributions in the piezoelectric layer.

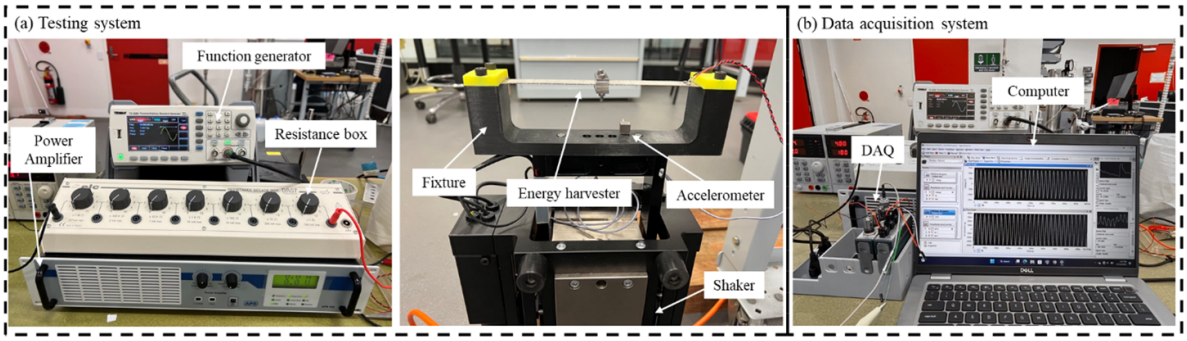

Figure 5. Experimental setup of the vibration energy harvesting test: (a) testing system; (b) data acquisition system.

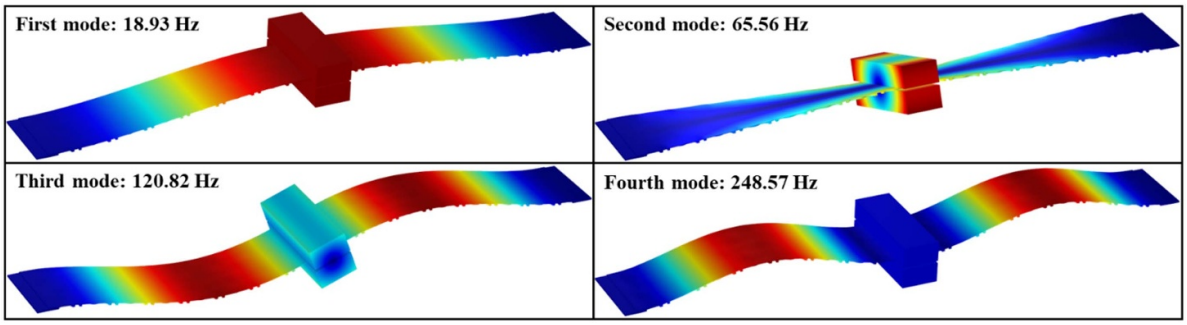

Figure 6. First four mode shapes of the AEH with a proof mass fixed at the beam centre.

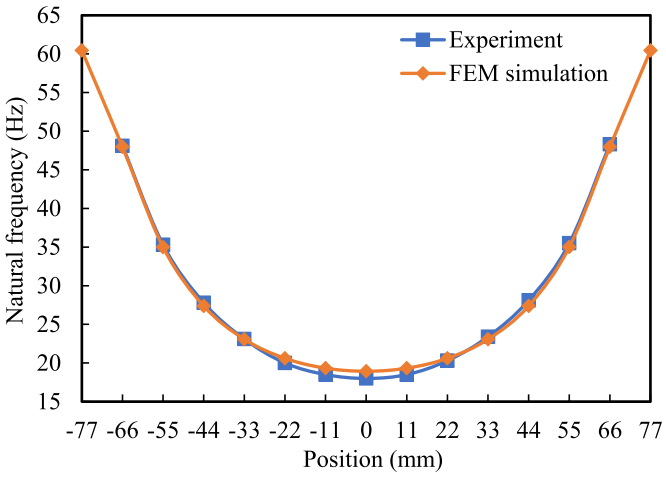

Figure 7. Experimental validation of natural frequencies of the AEH with a proof mass fixed at different positions.

To ensure a fair comparison, these simulations were performed for both PEH and AEH with a poof mass fixed at the centre of the beam under an excitation acceleration of 0.3 g at their respective first eigenfrequencies. Considering the structural symmetry of the two energy harvesters, the displacement and stress distributions of the piezoelectric beam are symmetrical with respect to the centre of the beam. Hence, only the displacement and stress distributions of the left half of the energy harvesters are depicted for comparison. As shown in figures 8(a) and (b), the longitudinal displacements of both substrates first increase and then decrease along the y-axis, which means that the regions near the fixed end undergo stretching, while the regions near the centre experience compression. The lateral displacement distribution of plain substrate (figure 8(c)) indicates that the plain substrate contracts laterally in the stretching region and expands laterally in the compression region, which aligns with the expected positive Poisson's ratio behaviour. In contrast, the auxetic substrate expands laterally in most regions (figure 8(d)). This behaviour arises because the longitudinal stress varies across the cross section of the substrate when it is in a bending mode, which is characterised by one surface in tension and the other in compression. The auxetic substrate consistently exhibits lateral expansion when both tensile and compressive stresses coexist within the auxetic substrate.

The stress distributions of piezoelectric films for the two energy harvesters are depicted in figures 8(e) and (f). It can be observed that the stress in the piezoelectric film of the AEH is higher than that of the PEH. To further evaluate the performance of the auxetic structure, the average strain and maximum stress in piezoelectric layers for both energy harvesters are summarised in table 3. For the piezoelectric film in the PEH, the average strains along the x axis ($\overline{\varepsilon_{xx}}$) and along the y axis ($\overline{\varepsilon_{yy}}$) have opposite signs, which means that $\overline{\varepsilon_{xx}}$ will diminish the power output generated by $\overline{\varepsilon_{yy}}$. In contrast, $\overline{\varepsilon_{xx}}$ and $\overline{\varepsilon_{yy}}$ in the piezoelectric layer of the AEH have the same signs, indicating that both stains can contribute to the power generation. Besides, the maximum stress in the piezoelectric film is 0.375 MPa for the PEH and 1.645 MPa for the AEH.

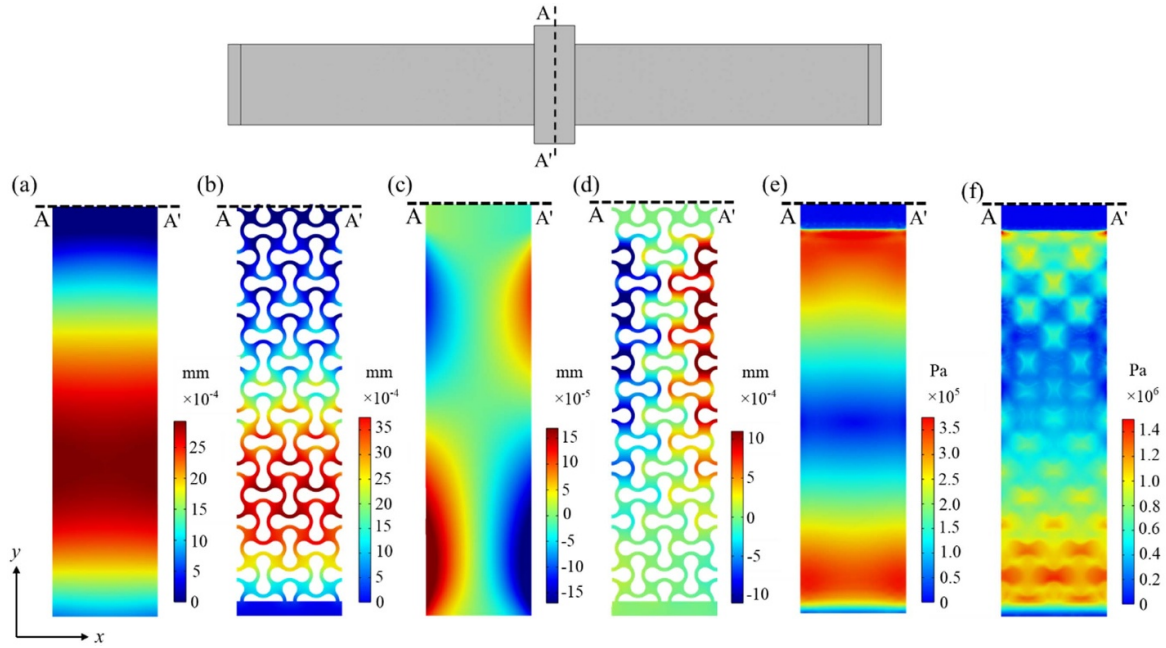

Figure 8. Displacement distributions of the left half of the substrate covered by the piezoelectric layer: along *y*-axis (a) plain structure and (b) auxetic structure; along *x*-axis: (c) plain structure and (d) auxetic structure; and stress distributions of the left half of the piezoelectric layer: (e) plain structure and (f) auxetic structure.

Table 3. Average strain and maximum stress in piezoelectric films.

Energy harvester	$\overline{\varepsilon_{xx}}$ (10^{-5})	$\overline{\varepsilon_{yy}}$ (10^{-5})	Maximum stress (MPa)
PEH	−0.328	1.891	0.375
AEH	1.093	3.866	1.645

To quantify the effect of the auxetic structure on vibration energy harvesting, the frequency responses of the AEH and the PEH were experimentally tested under an excitation acceleration of 0.3 g. The proof masses of both energy harvesters were fixed at the centre of the piezoelectric beam. The frequency responses of the energy harvesters were obtained through manual frequency sweep [17]. The excitation frequency was increased and decreased manually in steps of 0.5 Hz within the frequency ranges of interest. Considering that the AEH has a lower natural frequency compared to the PEH, the frequency range of interest for the AEH was defined as 15 Hz to 30 Hz, while the range for PEH was set as 30 Hz to 45 Hz. As shown in figure 9, the AEH achieves a maximum root mean square (RMS) output voltage of 2.07 V at a frequency of 25 Hz. In contrast, the PEH acquires a lower maximum RMS output voltage of 1.42 V at a frequency of 40 Hz. These results highlight the ability of the auxetic structure to enhance the voltage output of the energy harvester. Furthermore, obvious jump phenomena can be observed in the upward frequency responses of both energy harvesters. There also exist noticeable differences between upward and downward frequency responses as the structural stiffness varies with the vibration amplitude. These observations indicate the presence of geometric nonlinearity in the energy harvesters,

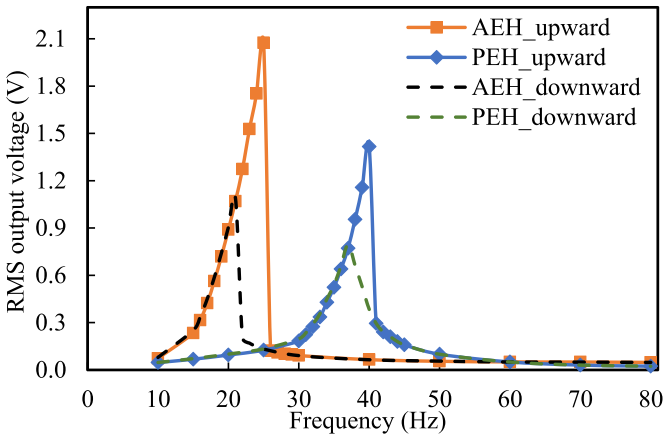

Figure 9. Comparison of the frequency responses of the AEH and the PEH under an excitation acceleration of 0.3 g.

which can be attributed to the occurrence of stretching strain in the doubly clamped beam under large vibration amplitudes.

4.3. Passive frequency self-tuning energy harvesting

For an AEH with a sliding proof mass, passive frequency self-tuning of the energy harvester can be achieved through the automatic movement of the sliding proof mass. To demonstrate the improved energy harvesting performance of the energy harvester, a series of experiments were conducted at different frequencies under a constant excitation acceleration of 0.3 g. Figures 10(a)–(d) depict the output voltage of the energy

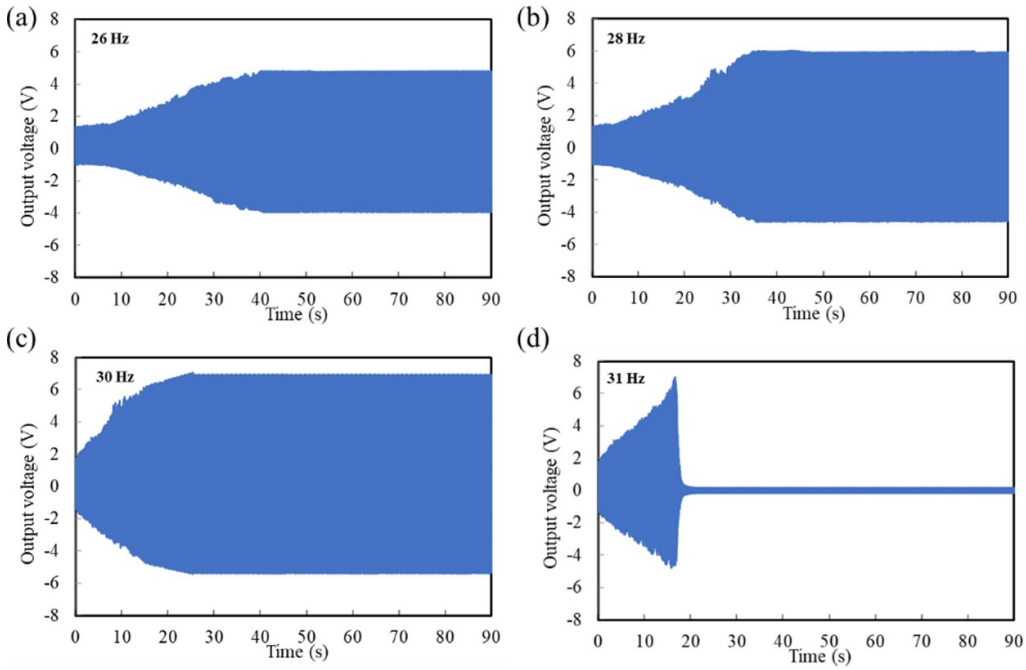

Figure 10. Time histories of the output voltage of the AEH with a sliding proof mass at different frequencies under a constant excitation acceleration of 0.3 g: (a) 26 Hz; (b) 28 Hz; (c) 30 Hz; (d) 31 Hz.

harvester over time at 26 Hz, 28 Hz, 30 Hz and 31 Hz, respectively. As shown in figure 10(a), when the energy harvester was subjected to an excitation frequency of 26 Hz, the initial output voltage of the energy harvester is relatively low owing to the small vibration amplitude of the piezoelectric beam. However, as the proof mass moves towards the beam centre, the output voltage gradually increases due to the amplified vibration amplitude. Ultimately, the output voltage of the energy harvester is significantly improved and remained constant, accompanied by the beam vibrating in a large amplitude and the proof mass anchored at a position near the beam centre. The transient responses of the energy harvester at 28 Hz (figure 10(b)) and 30 Hz (figure 10(c)) exhibit a similar trend as the case at 26 Hz. However, in the case of 31 Hz (figure 10(d)), the output voltage of the energy harvester increases dramatically at the beginning, followed by a sudden decrease. This behaviour may be attributed to the rapid movement of the proof mass, which may hinder the vibrating beam from effectively capturing the high vibration amplitude. Consequently, the nonlinear energy harvester transitions from the high-energy orbit to the low-energy orbit when the proof mass reaches the position near the centre. These results demonstrate that the sliding proof mass can automatically move from the side of the piezoelectric beam towards the beam centre to help the energy harvester capture high output voltage at different excitation frequencies within the frequency tuning range.

To investigate the effect of the initial position of the proof mass on frequency self-tuning, experiments were conducted with the sliding proof mass initially placed at three different positions. During the tests, the energy harvester was subjected to an excitation acceleration of 0.3 g at a constant frequency of 26 Hz. As shown in figure 11(a), when the initial position of the proof mass was 66 mm from the beam centre, the output voltage of the energy harvester consistently remains at an extremely low level. This is because the proof mass is kept at its initial position and the excited frequency is deviated from the resonance frequency of the structure, causing the beam to vibrate with a small vibration amplitude. The similar phenomenon was also discovered when the proof mass was initially placed at the beam centre, as shown in figure 11(c). The voltage output of the energy harvester is relatively low and remains unchanged over time. However, when the proof mass was initially placed at 44 mm from the beam centre, the energy harvester could realise frequency self-tuning to obtain high voltage output (figure 11(b)). These results imply that frequency self-tuning is only achieved when the proof mass is initially placed at an appropriate position. Specifically, the initial vibration amplitude of the piezoelectric beam should be sufficiently large to initiate the movement of the proof mass. Subsequently, the proof mass can autonomously move towards the beam centre to track the large vibration amplitude. Note that for the PEH under an excitation acceleration of 0.3 g, the proof mass cannot automatically move towards the beam centre regardless of its initial position. This may be attributed to the significantly higher stiffness of the plain substrate with smaller vibration amplitude in comparison to the auxetic substrate.

Figure 12 compares the RMS output voltage between the AEH with a fixed proof mass and the AEH with a sliding proof mass at different frequencies under a constant excitation acceleration of 0.3 g. In each test, the energy harvester remained in a stationary state until it was subjected to a specified excitation frequency. In the case of the AEH with a fixed proof

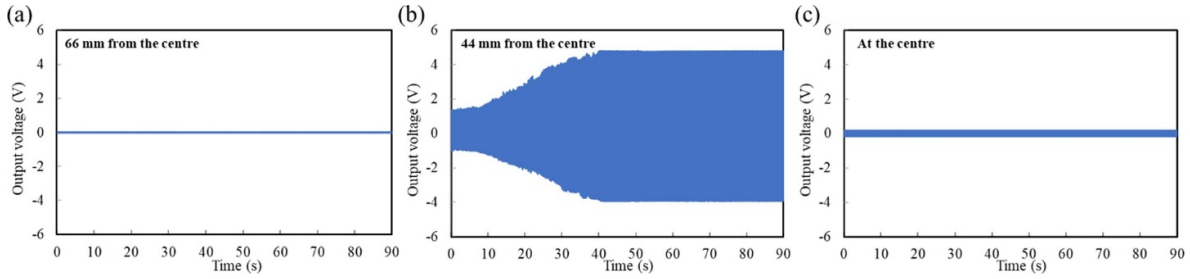

Figure 11. Time histories of the output voltage of the AEH with a sliding proof mass placed at different initial positions under an excitation acceleration of 0.3 g at 26 Hz: (a) 66 mm from the centre; (b) 44 mm from the centre; (c) at the centre.

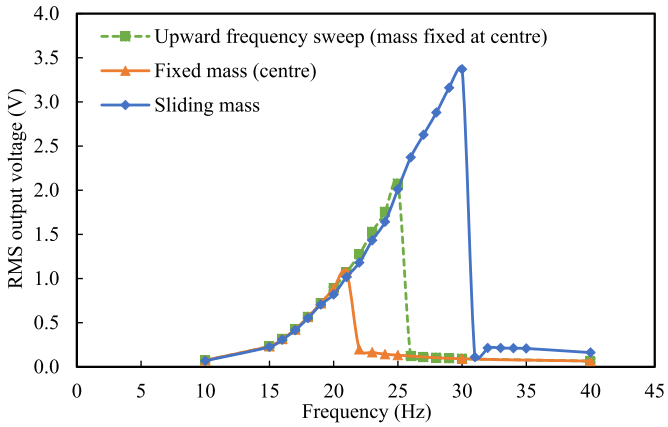

Figure 12. Comparison of the output voltage between the AEH with a fixed proof mass (centre) and the AEH with a sliding proof mass at different frequencies under an excitation acceleration of 0.3 g.

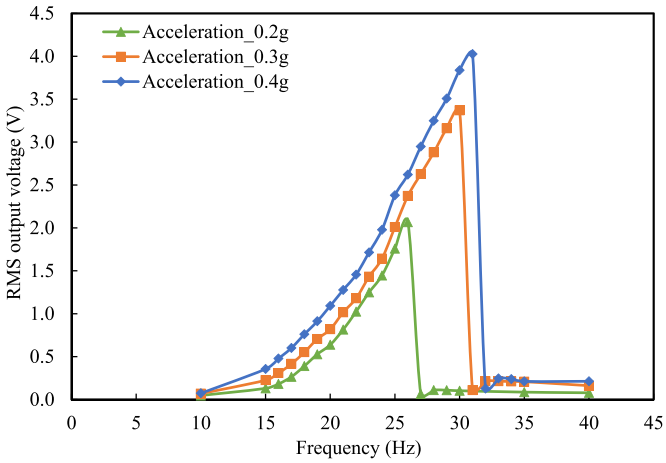

Figure 13. Output voltage of the AEH with a sliding proof mass under different excitation accelerations and frequencies.

mass, the proof mass was fixed at the beam centre to maximise output voltage. This configuration achieves a maximum RMS output voltage of 1.07 V at a frequency of 21 Hz. In contrast, the energy harvester with a sliding proof mass exhibits a maximum RMS output voltage of 3.37 V at a frequency of 30 Hz. Moreover, although the maximum RMS output voltage of the AEH with a fixed proof mass at the beam centre can be improved to 2.07 V at 25 Hz through the manual upward frequency sweep in steps of 0.5 Hz due to the occurrence of geometric nonlinearity, the AEH with a fixed proof mass at the beam centre exhibits a lower maximum operating frequency and RMS output voltage compared to the AEH with a sliding proof mass. Therefore, the introduction of the sliding proof mass significantly enhances the voltage output of AEH and broadens its working bandwidth by 9 Hz under an excitation acceleration of 0.3 g.

The RMS output voltage of the AEH with a sliding proof mass was investigated under different excitation accelerations and frequencies, as shown in figure 13. The RMS output voltage and maximum working frequency of the energy harvester increase with increasing acceleration because of the improved vibration amplitude of the piezoelectric beam over time. The increased vibration amplitude of the beam can enhance the geometry nonlinearity of the energy harvester. Thus, the high energy orbit of the energy harvester can be easily captured and maintained as the proof mass moves towards the beam centre. Furthermore, figure 14 depicts the time histories of the output voltage of the energy harvester during the frequency self-tuning process at a constant frequency of 26 Hz under three different excitation accelerations. To ensure a fair comparison, the initial position of the sliding mass remained consistent across these three tests, with a distance of 44 mm from the beam centre. It can be observed that transient response of the energy harvester under an excitation acceleration of 0.2 g is consistently much lower than that of the energy harvester under an excitation acceleration of 0.3 g and 0.4 g. This indicates that the piezoelectric beam consistently exhibits larger vertical displacement when subjected to higher excitation accelerations, resulting in stronger geometry nonlinearity.

4.4. Power output

To further evaluate the performance of the energy harvesters, the peak RMS output power for each energy harvester was examined with different load resistances under an excitation acceleration of 0.3 g, as shown in figure 15. Considering the energy harvester as a current source, the theoretical RMS power output generated by the energy harvester across the connected resistance can be calculated using equations (4)–(6) [57]. According to the experimental results, the PEH with a fixed proof mass has the lowest output power compared to the

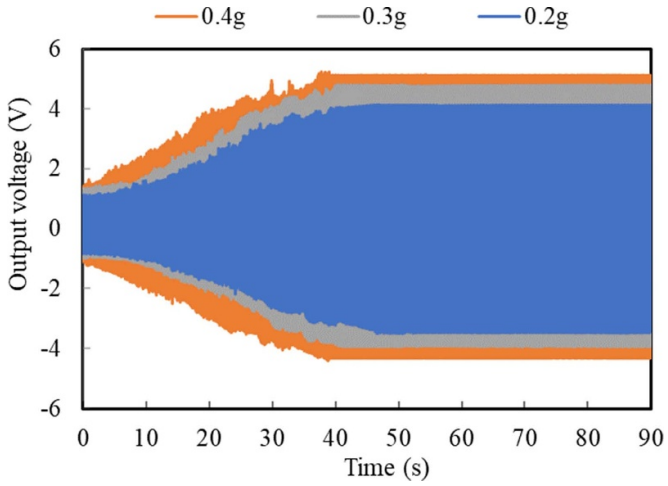

Figure 14. Time histories of the output voltage of the energy harvester with the moving mass at different accelerations under 26 Hz.

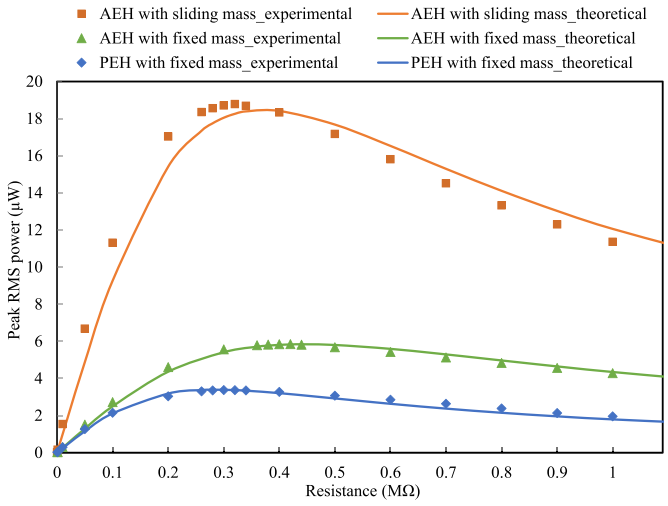

Figure 15. Peak RMS output power of the energy harvester with different load resistances under an excitation acceleration of 0.3 g.

other two PEHs. It achieves a maximum RMS output power of 3.37 μW at a load resistance of 300 kΩ. The AEH with a fixed proof mass demonstrates a higher maximum RMS power output of 5.85 μW at a load resistance of 420 kΩ. The AEH with a sliding proof mass exhibits the highest output power, reaching a maximum RMS power output of 18.78 μW when connected to a load resistance of 320 kΩ. This value is 2.21 times higher than that of the AEH with a fixed proof mass and 4.57 times higher than that of the PEH with a fixed proof mass. In conclusion, the auxetic structure can improve the power output of the energy harvester, and the introduction of the sliding proof can further improve the working bandwidth and power output of the energy harvester due to its frequency self-tuning capability

$$P = \frac{U_R \times I_R}{2} \tag{4}$$

$$U_R = R \times I_R \tag{5}$$

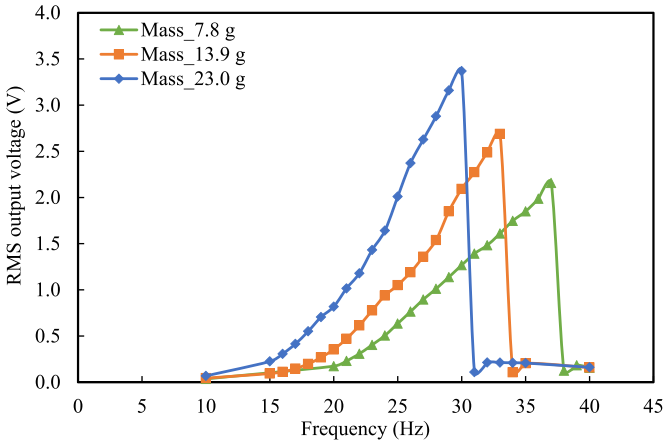

Figure 16. Output voltage of the AEH with a sliding proof mass of different weights under an excitation acceleration of 0.3 g.

$$I_R = \frac{I_0}{\sqrt{1 + R^2 C^2 \omega^2}} \tag{6}$$

where P, U_R, I_R denotes the RMS power output, voltage amplitude, and current amplitude across the connected resistance load resistance R, respectively. I_0 denotes the short-circuit current generated by the energy harvester, which can be measured in the experiments. C denotes the capacitance of the piezoelectric film, with a value of approximately 14.8 pF, ω denotes the angular frequency of the external excitation applied to the energy harvester.

4.5. Parametric studies for the sliding mass

Since the proof mass exhibits a significant impact on vibration energy harvesting, the influence of the weight and the gap size of the sliding proof mass on the performance of the energy harvester was experimentally investigated. As shown in figure 16, with the increase in the weight of the sliding proof mass, the working frequencies of the energy harvester shift from the high frequencies to low frequencies. At the same time, the RMS output voltage of the energy harvester increases as the weight of the proof mass increases. This is because a heavier proof mass results in a larger vibration amplitude of the piezoelectric beam when the sliding proof mass stabilises near the beam centre.

In addition, the transient responses of the AEH with a sliding proof mass of various gap sizes during the frequency self-tuning process were investigated. The experiments were conducted under an excitation acceleration of 0.3 g at a frequency of 26 Hz with the sliding proof mass initially placed at 44 mm from the beam centre. As shown in figure 17, the energy harvester with a sliding proof mass of a smaller gap size exhibits a slightly lower output voltage, and it takes more time for the proof mass to move towards the beam centre during the frequency self-tuning process with the decrease of the gap size. This behaviour can be attributed to the increase in the friction force and impacts between the sliding proof mass

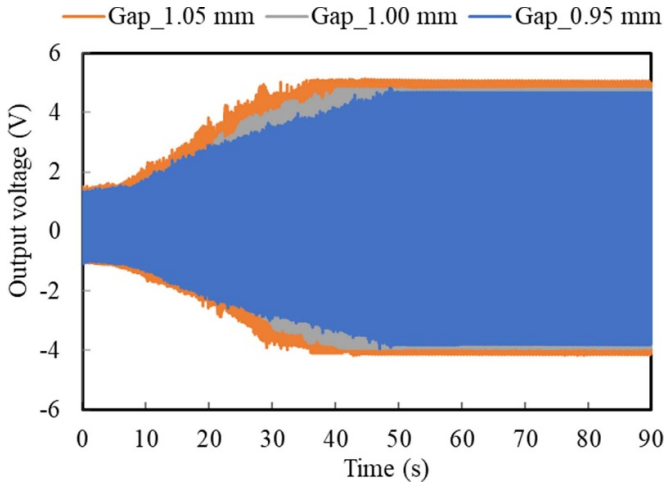

Figure 17. Time histories of the output voltage of the AEH with a sliding proof mass of different gap sizes under an excitation acceleration of 0.3 g at 26 Hz.

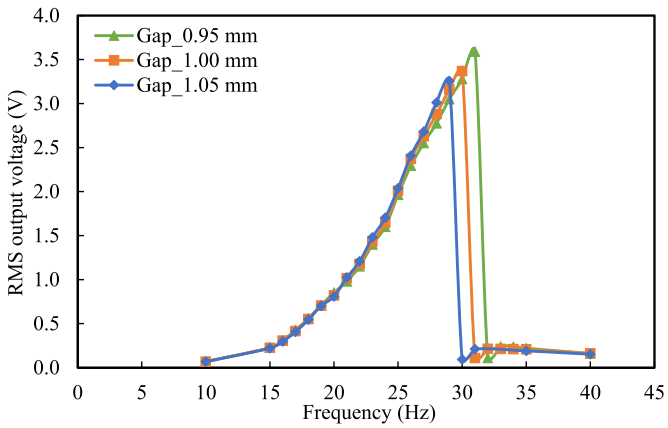

Figure 18. Output voltage of the AEH with a sliding proof mass of different gap size at different frequencies under an excitation acceleration of 0.3 g.

and the vibrating beam, which slows down the movement of the sliding proof mass. Furthermore, figure 18 shows the RMS output voltage of the AEH with a sliding proof mass of different gap sizes as a function of excitation frequency under an excitation acceleration of 0.3 g. The gap size of the proof mass has little impact on the RMS output voltage of the energy harvester under the same excitation frequency within the frequency self-tuning range. However, a slight increase in the maximum working frequency of the energy harvester is observed as the gap size of the sliding proof mass decreases.

5. Practical applications

With the prevalence of mine IoT, a wide range of sensors have been extensively deployed in mine sites for environmental monitoring and production management [58]. However, as the number of sensors at mine sites continues to rise dramatically, the use of cable-based sensors becomes impractical due to the complexity and high cost of cable deployment and maintenance [59]. To address this issue, vibration energy harvesters can be employed in mine environments to harness vibration energy from operating machinery and power the nearby sensors. The feasibility of the developed piezoelectric energy harvester for mining applications was evaluated based on the vibration produced by a centrifuge in the coal handling and preparation plant (CHPP). According to figure 19(a), the centrifuge can generate sufficient and stable vibrations for vibration energy harvesting, exhibiting an RMS acceleration of 0.346 g. The dominant frequency of the measured acceleration is 25.0 Hz, which is within the working bandwidth of the proposed energy harvester figure 19(b).

To demonstrate the potential of the proposed energy harvester for powering IoT devices, laboratory experiments were conducted. The applied vibration to the energy harvester in these experiments replicates the dominant frequency and amplitude of the vibrations produced by a centrifuge at the CHPP. The developed energy harvester was connected with a commercial IoT device kit (Cypress S6SAE101A00SA1002) to show its capability in powering a Bluetooth low energy (BLE) beacon and a wireless humidity and temperature sensor node. The IoT device kit consists of an energy harvesting motherboard and a BLE-USB bridge. The motherboard includes two diode bridges to convert the generated AC voltage into DC voltage, a power management integrated circuit with an extremely low start-up power (1.2 μW) to manage and control the power supply, a humidity and temperature sensor for environmental monitoring, and a BLE module to enable wireless communication. As shown in figure 20, the energy harvester captured vibration energy from the shaker. The generated AC power was then rectified by diode bridges and stored in a capacitor. Subsequently, the stored energy was utilised to power the electronics on motherboard.

In the experiments, the developed energy harvester consistently generated an RMS output voltage of 2.297 V when the sliding mass stabilised on the beam under an excitation acceleration of 0.346 g at 25 Hz. Since the motherboard can function as either a BLE beacon or a humidity and temperature sensor node, two types of experiments were conducted. For powering the BLE beacon, a capacitor with a capacitance of 47 μF was used as an external storage component. Figure 21 illustrates the charge and discharge curve of the capacitor while powering a BLE beacon. Initially, as the power generated by the energy harvester gradually accumulates in the capacitor, the voltage across the capacitor gradually increases. Once the voltage reaches 3.28 V, the motherboard wakes up, and the BLE beacon begins broadcasting its unique identifier. This causes a sharp decrease in the voltage across the capacitor. The identifier can be detected by the BLE-USB bridge and read by the computer. When the voltage drops to 1.92 V, the motherboard goes back to sleep mode until the voltage across the capacitor returns to 3.28 V. In

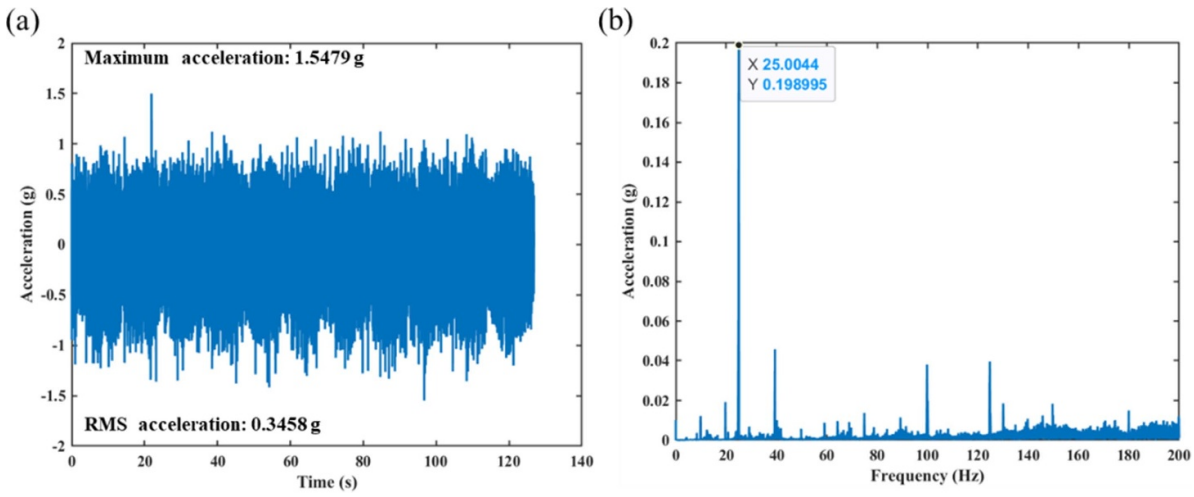

Figure 19. Vibration data collected from a centrifuge along the z axis: (a) time history signal of the measured acceleration; and (b) frequency distribution of the measured acceleration.

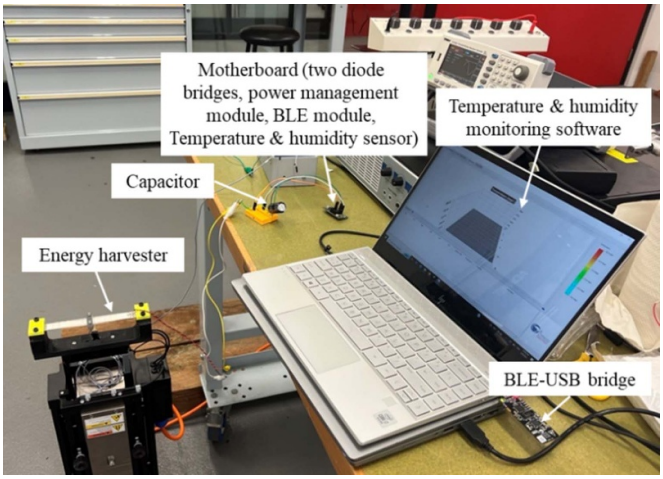

Figure 20. Experimental setup of vibration energy harvesting for powering a sensor node.

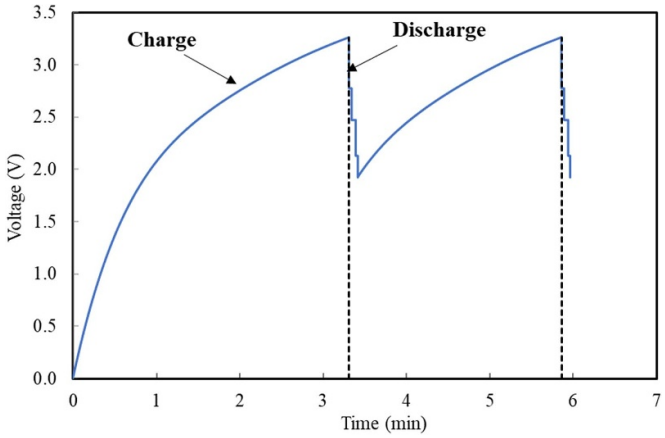

Figure 21. Charge and discharge curve of the capacitor while powering a BLE beacon.

general, the energy harvester enables BLE beacon to broadcast its identifier at intervals of approximately 2 min and 40 s.

To power the temperature and humidity sensor node, a capacitor with a capacitance of 100 μF was applied to storage the power generated by the vibration energy harvester.

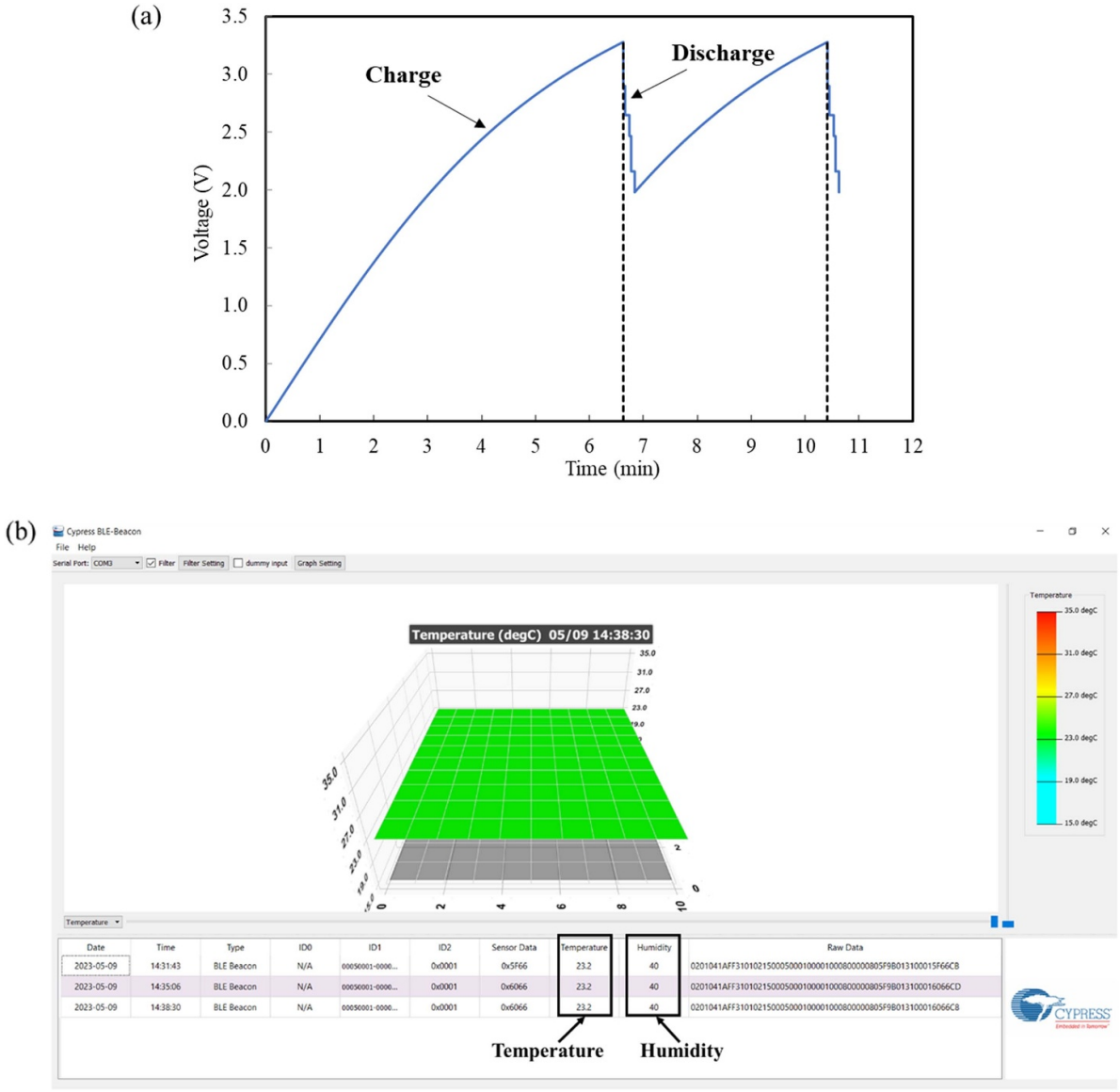

Figure 22. VEH for powering a temperature and humidity sensor node: (a) charge and discharge curve of the capacitor; and (b) temperature and humidity data recorded by the self-powered sensor node.

As shown in figure 22(a), initially, it takes approximately 6 min and 40 s to charge the capacitor, allowing the voltage across the capacitor to reach 3.3 V. Afterwards, the capacitor discharges to power the sensor node until its voltage decreases to 1.98 V. During this period, the temperature and humidity sensor measures the surrounding temperature and humidity once. The collected data is then transmitted to the BLE-USB bridge through BLE connectivity and recorded by the monitoring software (figure 22(b)). The temperature and humidity data can be monitored every 3 min and 30 s. Therefore, the developed piezoelectric energy harvester can harvest sufficient vibration energy from the centrifuge to periodically power a BLE beacon or a sensor node at the mine site.

6. Conclusion

An auxetic piezoelectric energy harvester with frequency self-tuning capability was developed for efficient and broadband vibration energy harvesting. The auxetic structures effectively reduces the natural frequency and increases the output power of the energy harvester simultaneously. The sliding proof mass with an appropriate initial position can automatically adjust its position along the vibrating doubly clamped beam to modulate the dynamic response of the system and capture the high vibration amplitude of the beam across a range of frequencies. FEM is conducted to analyse the effect of the auxetic structure and the position of the proof mass on the characteristics of the energy harvester, which is consistent

with the experimental results. Experiments are performed to investigate the improved energy harvesting performance of the proposed energy harvester. Under an excitation acceleration of 0.3 g, the introduction of the sliding proof mass widens the working bandwidth of the AEH by 9 Hz (from 21 Hz to 30 Hz). Besides, due to the geometry nonlinearity of the doubly clamped beam under large vibration amplitudes, the AEH with a sliding mass has the highest maximum output power compared to PEH and AEH with a fixed proof mass. The maximum RMS output power of AEH with a sliding mass reaches 18.78 μW under 0.3 g excitation acceleration, which is 2.21 times higher than that of the AEH with a fixed proof mass and 4.57 times higher than that of the PEH with a fixed proof mass. Additionally, the results of the parametric studies indicate the weight of the sliding proof mass has a significant impact on energy harvesting performance, while the gap size of the sliding proof mass exhibits little influence. Furthermore, the developed energy harvester has successfully demonstrated its potential to power either a BLE beacon or a temperature and humidity sensor node in real-world mine environments. We believe that this study will provide guidance for the design of more efficient piezoelectric energy harvesters to realise self-powered IIoT sensors.

Data availability statement

The data belong to the ARACP project and UNSW. The data cannot be made publicly available upon publication because they are owned by a third party and the terms of use prevent public distribution. The data that support the findings of this study are available upon reasonable request from the authors.

Acknowledgments

The authors gratefully acknowledge support from the Australian Coal Industry's Research Program—Project C33033.

Conflict of interest

The authors declare that they have no known competing financial interests or personal relationships that could have appeared to influence the work reported in this paper.

ORCID iD

Huili Zhang https://orcid.org/0000-0003-2051-5426

References

[1] Qin W, Chen S and Peng M 2020 Recent advances in industrial internet: insights and challenges *Digit. Commun. Netw.* **6** 1–13
[2] Sisinni E, Saifullah A, Han S, Jennehag U and Gidlund M 2018 Industrial internet of things: challenges, opportunities, and directions *IEEE Trans. Ind. Inform.* **14** 4724–34
[3] Zhang L, Zhang F, Qin Z, Han Q, Wang T and Chu F 2022 Piezoelectric energy harvester for rolling bearings with capability of self-powered condition monitoring *Energy* **238** 121770
[4] Aabid A, Raheman M A, Ibrahim Y E, Anjum A, Hrairi M, Parveez B, Parveen N and Mohammed Zayan J 2021 A systematic review of piezoelectric materials and energy harvesters for industrial applications *Sensors* **21** 4145
[5] Liu H, Zhong J, Lee C, Lee S-W and Lin L 2018 A comprehensive review on piezoelectric energy harvesting technology: materials, mechanisms, and applications *Appl. Phys. Rev.* **5** 041306
[6] Maamer B, Boughamoura A, El-Bab A M F, Francis L A and Tounsi F 2019 A review on design improvements and techniques for mechanical energy harvesting using piezoelectric and electromagnetic schemes *Energy Convers. Manage.* **199** 111973
[7] Wei C and Jing X 2017 A comprehensive review on vibration energy harvesting: modelling and realization *Renew. Sustain. Energy Rev.* **74** 1–18
[8] Song H-C, Kumar P, Maurya D, Kang M-G, Reynolds W T, Jeong D-Y, Kang C-Y and Priya S 2017 Ultra-low resonant piezoelectric MEMS energy harvester with high power density *J. Microelectromech. Syst.* **26** 1226–34
[9] Li Z, Zhao L, Wang J, Yang Z, Peng Y, Xie S and Ding J 2023 Piezoelectric energy harvesting from extremely low-frequency vibrations via gravity induced self-excited resonance *Renew. Energy* **204** 546–55
[10] Song H-C *et al* 2018 Broadband dual phase energy harvester: vibration and magnetic field *Appl. Energy* **225** 1132–42
[11] Twiefel J and Westermann H 2013 Survey on broadband techniques for vibration energy harvesting *J. Intell. Mater. Syst. Struct.* **24** 1291–302
[12] Toyabur R M, Salauddin M and Park J Y 2017 Design and experiment of piezoelectric multimodal energy harvester for low frequency vibration *Ceram. Int.* **43** S675–81
[13] El-Hebeary M M R, Arafa M H and Megahed S M 2013 Modeling and experimental verification of multi-modal vibration energy harvesting from plate structures *Sens. Actuators* **193** 35–47
[14] Stanton S C, McGehee C C and Mann B P 2009 Reversible hysteresis for broadband magnetopiezoelastic energy harvesting *Appl. Phys. Lett.* **95** 174103
[15] Chen Y and Yan Z 2020 Nonlinear analysis of axially loaded piezoelectric energy harvesters with flexoelectricity *Int. J. Mech. Sci.* **173** 105473
[16] Xu C, Liang Z, Ren B, Di W, Luo H, Wang D, Wang K and Chen Z 2013 Bi-stable energy harvesting based on a simply supported piezoelectric buckled beam *J. Appl. Phys.* **114** 114507
[17] Fan K, Zhang Y, Liu H, Cai M and Tan Q 2019 A nonlinear two-degree-of-freedom electromagnetic energy harvester for ultra-low frequency vibrations and human body motions *Renew. Energy* **138** 292–302
[18] Chen K, Ding X, Tian L, Shen H, Song R, Bian Y and Yang Q 2023 An M−shaped buckled beam for enhancing nonlinear energy harvesting *Mech. Syst. Signal Process.* **188** 110066
[19] Li H, Sun H, Song B, Zhang D, Shang X and Liu D 2021 Nonlinear dynamic response of an L-shaped beam-mass piezoelectric energy harvester *J. Sound Vib.* **499** 116004
[20] Fan Y, Zhang Y, Niu M-Q and Chen L-Q 2024 An internal resonance piezoelectric energy harvester based on geometrical nonlinearities *Mech. Syst. Signal Process.* **211** 111176
[21] Qian F, Hajj M R and Zuo L 2020 Bio-inspired bi-stable piezoelectric harvester for broadband vibration energy harvesting *Energy Convers. Manage.* **222** 113174
[22] Zou D, Liu G, Rao Z, Tan T, Zhang W and Liao W-H 2021 A device capable of customizing nonlinear forces for vibration

energy harvesting, vibration isolation, and nonlinear energy sink *Mech. Syst. Signal Process.* **147** 107101
[23] Wang T, Zhang Q, Han J, Wang W, Yan Y, Cao X and Hao S 2023 Bio-inspired quad-stable piezoelectric energy harvester for low-frequency vibration scavenging *Energy* **282** 128952
[24] Lallart M, Anton S R and Inman D J 2010 Frequency self-tuning scheme for broadband vibration energy harvesting *J. Intell. Mater. Syst. Struct.* **21** 897–906
[25] Peters C, Maurath D, Schock W, Mezger F and Manoli Y 2009 A closed-loop wide-range tunable mechanical resonator for energy harvesting systems *J. Micromech. Microeng.* **19** 094004
[26] Heller S, Neiss S, Kroener M and Woias P 2015 Self-sufficient electronic control for nonlinear, frequency tunable, piezoelectric vibration harvesters *J. Phys.: Conf. Ser.* **660** 012024
[27] Cheng Y, Wu N and Wang Q 2017 An efficient piezoelectric energy harvester with frequency self-tuning *J. Sound Vib.* **396** 69–82
[28] Yan L, Lallart M and Karami A 2019 Low-cost orbit jump in nonlinear energy harvesters through energy-efficient stiffness modulation *Sens. Actuators* **285** 676–84
[29] Deng L, Jiang J, Zhang D, Zhou L and Fang Y 2021 Design and modeling a frequency self-tuning vibration energy harvester for rotational applications *Energy* **235** 121414
[30] Lan C, Chen Z, Hu G, Liao Y and Qin W 2021 Achieve frequency-self-tracking energy harvesting using a passively adaptive cantilever beam *Mech. Syst. Signal Process.* **156** 107672
[31] Yu L, Tang L and Yang T 2020 Piezoelectric passive self-tuning energy harvester based on a beam-slider structure *J. Sound Vib.* **489** 115689
[32] Yu L, Tang L and Yang T 2019 Experimental investigation of a passive self-tuning resonator based on a beam-slider structure *Acta Mech. Sin.* **35** 1079–92
[33] Miller L M, Pillatsch P, Halvorsen E, Wright P K, Yeatman E M and Holmes A S 2013 Experimental passive self-tuning behavior of a beam resonator with sliding proof mass *J. Sound Vib.* **332** 7142–52
[34] Shin Y-H, Choi J, Kim S J, Kim S, Maurya D, Sung T-H, Priya S, Kang C-Y and Song H-C 2020 Automatic resonance tuning mechanism for ultra-wide bandwidth mechanical energy harvesting *Nano Energy* **77** 104986
[35] Baker J, Roundy S and Wright P 2005 Alternative geometries for increasing power density in vibration energy scavenging for wireless sensor networks *3rd Int. Energy Conversion Engineering Conf.* (American Institute of Aeronautics and Astronautics) (https://doi.org/10.2514/6.2005-5617)
[36] Dietl J M and Garcia E 2010 Beam shape optimization for power harvesting *J. Intell. Mater. Syst. Struct.* **21** 633–46
[37] Ayed S B, Abdelkefi A, Najar F and Hajj M R 2014 Design and performance of variable-shaped piezoelectric energy harvesters *J. Intell. Mater. Syst. Struct.* **25** 174–86
[38] Li Q, Kuang Y and Zhu M 2017 Auxetic piezoelectric energy harvesters for increased electric power output *AIP Adv.* **7** 015104
[39] Tabak A, Safaei B, Memarzadeh A, Arman S and Kizilors C 2023 An extensive review of piezoelectric energy-harvesting structures utilizing auxetic materials *J. Vib. Eng. Technol.* 1–38
[40] Ebrahimian F, Kabirian Z, Younesian D and Eghbali P 2021 Auxetic clamped-clamped resonators for high-efficiency vibration energy harvesting at low-frequency excitation *Appl. Energy* **295** 117010
[41] Sadikbasha S, Radhika B and Pandurangan V 2022 Auxetic hexachiral cantilever beams for piezoelectric vibration energy harvesting *Smart Mater. Struct.* **31** 105015
[42] Fang S, Du H, Yan T, Chen K, Li Z, Ma X, Lai Z and Zhou S 2024 Theoretical and experimental investigation on the advantages of auxetic nonlinear vortex-induced vibration energy harvesting *Appl. Energy* **356** 122395
[43] Tikariha A K, Saurabh N, Gudipadu V and Patel S 2022 Effect of auxetic structures parameters variation on PVDF-based piezoelectric energy harvesters *J. Appl. Phys.* **132** 244105
[44] Xie J, Xu Y, Wan Z, Ghaderiaram A, Schlangen E and Šavija B 2023 Auxetic cementitious cellular composite (ACCC) PVDF-based energy harvester *Energy Build.* **298** 113582
[45] Chen K, Gao Q, Fang S, Zou D, Yang Z and Liao W-H 2021 An auxetic nonlinear piezoelectric energy harvester for enhancing efficiency and bandwidth *Appl. Energy* **298** 117274
[46] Chen K, Fang S, Gao Q, Zou D, Cao J and Liao W-H 2022 An enhanced nonlinear piezoelectric energy harvester with multiple rotating square unit cells *Mech. Syst. Signal Process.* **173** 109065
[47] Chen K, Fang S, Gao Q, Zou D, Cao J and Liao W-H 2022 Enhancing power output of piezoelectric energy harvesting by gradient auxetic structures *Appl. Phys. Lett.* **120** 103901
[48] Zhao B, Wang J, Hu G, Colombi A, Liao W-H and Liang J 2023 Time-sharing orbit jump and energy harvesting in nonlinear piezoelectric energy harvesters using a synchronous switch circuit *Mech. Syst. Signal Process.* **200** 110601
[49] Wang J and Liao W-H 2019 Attaining the high-energy orbit of nonlinear energy harvesters by load perturbation *Energy Convers. Manage.* **192** 30–36
[50] Zhou S, Cao J, Inman D J, Liu S, Wang W and Lin J 2015 Impact-induced high-energy orbits of nonlinear energy harvesters *Appl. Phys. Lett.* **106** 093901
[51] Wang H, Zhang Y, Lin W and Qin Q-H 2020 A novel two-dimensional mechanical metamaterial with negative Poisson's ratio *Comput. Mater. Sci.* **171** 109232
[52] Sezer N and Koç M 2021 A comprehensive review on the state-of-the-art of piezoelectric energy harvesting *Nano Energy* **80** 105567
[53] Khazaee M, Rezaniakolaie A, Moosavian A and Rosendahl L 2019 A novel method for autonomous remote condition monitoring of rotating machines using piezoelectric energy harvesting approach *Sens. Actuators* **295** 37–50
[54] Yu L, Tang L, Xiong L, Yang T and Mace B R 2019 A passive self-tuning nonlinear resonator with beam-slider structure *Proc. SPIE* **10967** 122–9
[55] Kim H, Smith A, Barry O and Zuo L 2019 Self-resonant energy harvester with a passively tuned sliding mass *Dynamic Systems and Control Conf.* (American Society of Mechanical Engineers Digital Collection vol 2) (https://doi.org/10.1115/DSCC2019-9000)
[56] Eghbali P, Younesian D and Farhangdoust S 2020 Enhancement of piezoelectric vibration energy harvesting with auxetic boosters *Int. J. Energy Res.* **44** 1179–90
[57] Le Scornec J, Guiffard B, Seveno R, Le Cam V and Ginestar S 2022 Self-powered communicating wireless sensor with flexible aero-piezoelectric energy harvester *Renew. Energy* **184** 551–63
[58] Zhang H, Li B, Karimi M, Saydam S and Hassan M 2023 Recent advancements in IoT implementation for environmental, safety, and production monitoring in underground mines *IEEE Internet Things J.* **10** 14507–26
[59] Mishra P K, Kumar S, Pratik, Kumar M and Kumar J 2019 IoT based multimode sensing platform for underground coal mines *Wirel. Pers. Commun.* **108** 1227–42